TWO-DIMENSIONAL DIFFRACTION TOMOGRAPHIC ALGORITHM FOR THROUGH-THE-WALL RADAR IMAGING

W. J. Zhang* and A. Hoorfar

Antenna Research Laboratory, Center for Advanced Communications, Villanova University, Villanova, PA 19085, USA

Abstract—In this paper, a two-dimensional (2D) diffraction tomographic algorithm based on the first order Born approximation is proposed for the imaging of hidden targets behind the wall. The spectral expansion of the three layered background medium Green's function is employed to derive a linear relationship between the spatial Fourier transforms of the image and the received scattered field. Then the image can be efficiently reconstructed with inverse Fast Fourier Transform (IFFT). The linearization of the inversion scheme and the easy implementation of the algorithm with FFT/IFFT make the diffraction tomographic algorithm suitable in through-the-wall radar imaging (TWRI) applications concerning the diagnostics of large probed domain and allow real-time processing. Numerical and experimental results are provided to show the effectiveness and high efficiency of the proposed diffraction tomographic algorithm for TWRI.

1. INTRODUCTION

The capability of electromagnetic (EM) wave to penetrate through building walls has made through-the-wall radar imaging (TWRI) of increasing importance in a wide range of both civilian and military applications. Search-and-rescue workers, urban-warfare specialists, and counter-terrorism agents often encounter situations where they need to detect, locate, and identify the hidden targets behind the visually opaque building walls. TWRI provides an efficient means for meeting these needs when the entering of a room or a building is considered to be hazardous or impossible [1–6].

Through-the-wall radar images the targets behind the wall by transmitting ultrawideband EM waves and processing the reflected

signal from the wall and the targets. Previously, several effective
TWRI algorithms that take into account the wave reflection, bending,
and delay effects due to the presence of the wall have been proposed
in [1, 2, 7–11]. These algorithms can be generally grouped into two
main categories. The first category is the noncoherent approach
based on the trilateration technique [7]. The noncoherent approach
is mainly used for target localization and is difficult to deal with
multi-target scenarios. The second category is the coherent algorithms
which are generally based on the coherent processing of the received
data [1, 2, 8–11]. Coherent algorithms can provide high range and
azimuth resolution imaging result of the targets and are extensively
studied in recent years. The beamforming algorithm based on the
delay-and-sum (DS) of the received signal for TWRI is proposed
in [8]. The effects of EM wave propagation through dielectric walls,
such as refraction and propagation delay, were incorporated into the
beamformer through ray tracing technique. In order to build an
accurate EM model for TWRI, the Contrast Source Inversion (CSI)
method is employed in [10]. CSI does not make any assumption of
the TWRI problem thus very high resolution image can be achieved.
However, this is a nonlinear optimization algorithm and needs to
be solved iteratively thus is very time consuming. Linear inverse
scattering algorithms based on the first order Born approximation,
which compensate for the wall effect through the efficiently exact or
approximate evaluation of the layered medium Green's function, were
proposed in [1, 9]. Linear inverse scattering TWRI algorithms show a
good improvement over CSI in the view of computation speed. For
multistatic radar systems, subspace method based on time reversal
multiple signal classification (TR-MUSIC) is proposed to detect and
localize targets behind the wall in [11].

    Although successful imaging results can been achieved by the
aforementioned TWRI algorithms, all these algorithms are based on
pixel-by-pixel reconstruction of the image, making them still not
applicable for real time processing. The imaging time increases
significantly with the increasing of number of pixels of the image. In
TWRI applications, a long data processing time should be avoided
in order to achieve a real time tracking of the targets behind the
wall. TWRI algorithms must be computationally efficient, so that
the location of the targets can be determined in a few seconds
with a portable computer. Linearized inversion schemes based
on diffraction tomography (DT) require much less computational
resources and are particularly well suited for on-site application due
to the easy implementation of the algorithm with Fast/inverse Fast
Fourier Transform (FFT/IFFT). DT was first proposed by Wolf in [12]

and is now widely used in various forms for such applications as medical imaging, optical imaging, geophysical tomography and radar imaging [15–20]. The principle of DT is based on the derivation of a linear relation between the spatial Fourier transform of the contrast function and the scattered field for weak scatterers [13–17]. A generalized DT algorithm for multi-frequency multi-monostatic Ground Penetrating Radar (GPR) measurement configuration was first proposed by Deming and Devaney in [13]. By employing first order Born approximation, the contrast function is estimated analytically by inverting a set of coupled equations using the regularized pseudo-inverse operator. Novel DT algorithms that take into account the air-ground interface for two/three-dimensional (2D/3D) buried targets imaging under lossy earth were proposed by Cui and Chew in [15, 16]. Most of the related works on DT were originally focused on freespace synthetic aperture radar (SAR) imaging [19, 20] and later on subsurface imaging. However, many practical applications, both military and commercial, are in the scenarios with target hidden behind an inaccessible obstacle, such as in through wall target detection and localization. Therefore, it is beneficial to carry out the study and develop DT algorithm for TWRI. In this paper, a 2D DT algorithm based on the first order Born approximation is proposed for TWRI. The spectral expansion of the three layered background medium Green's function is employed to derive a linear relation between the spatial Fourier transforms of the image and the scattered field. Then the image can be efficiently reconstructed with IFFT. The linearization of the inversion scheme and employment of FFT/IFFT in the imaging formula make the DT TWRI algorithm suitable for on-site applications. Numerical and experimental results are provided to show the effectiveness and high efficiency of the proposed DT TWRI algorithm.

The organization of the remainder of the paper is listed as follows. In Section 2, the formulation of the 2D DT algorithm for the imaging of targets behind the wall is presented. In Section 3, numerical and experimental results are provided to show the effectiveness and efficiency of the proposed DT algorithm for TWRI. Finally, some concluding remarks are drawn in Section 4.

2. DIFFRACTION TOMOGRAHPIC TWRI

Figure 1 shows a typical scenario of TWRI using the monostatic synthetic aperture radar (SAR). In this paper we consider the 2D problem where both the wall and target are assumed to be infinitely long and invariance along the y-axis. As is shown in Figure 1,
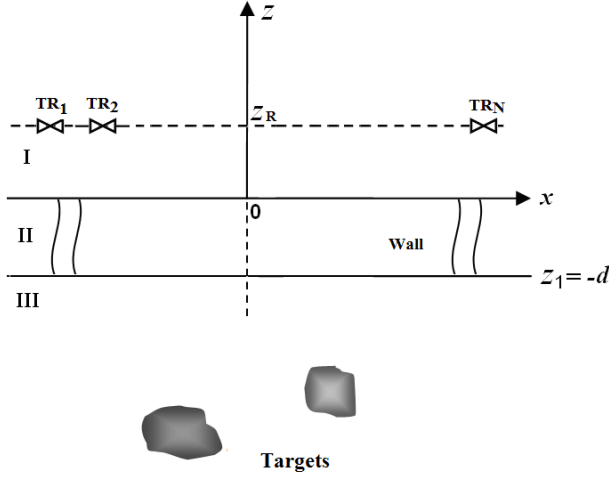
Figure 1. Measurement configuration of TWI.

the background medium consists of three regions: Region I and III are freespace and Region II is the wall whose relative permittivity, conductivity and thickness are denoted as ε_b, σ_b and d, respectively. The targets are located in an inaccessible investigated region denoted as D_{inv} behind the wall in Region III. The transceiver moves along a scan line parallel to the wall in x direction at a standoff distance z_R in Region I. The working frequency of the transmitter and receiver ranges from $f_{\min}$ to $f_{\max}$.

Assume that the electric current is a 2D point source, which is equivalent to a three-dimensional (3D) line source directed in the y direction. In this case only the y component of the electric field is nonzero and the subscript y will be omitted in the following formulations. Then the scattered electric field from targets observed at the receiver location can be written as

$$E_s\left(\rho_R, k\right) = k^2 \int_{D_{inv}} G\left(\rho_R, \rho, k\right) E_t\left(\rho, \rho_T, k\right) \mathrm{O}\left(\rho\right) d\rho \qquad (1)$$

where k is the wavenumber in the free space, ρ_T, ρ_R, and ρ are the position vectors of the transmitter, receiver and target, respectively, $\rho_T = \hat{\mathbf{x}} x_T + \hat{\mathbf{z}} z_T$, $\rho_R = \hat{\mathbf{x}} x_R + \hat{\mathbf{z}} z_R$, and $\rho = \hat{\mathbf{x}} x + \hat{\mathbf{z}} z$. $G(\rho_R, \rho, k)$ is the Green's function for the background layered medium, $E_t(\rho, \rho_T, k)$ is the total electrical field inside the target. $\mathrm{O}(\rho)$ is the contrast function of the target defined as

$$\mathrm{O}\left(\rho\right) = \tilde{\varepsilon}_r\left(\rho\right) - 1 \qquad (2)$$

where $\tilde{\varepsilon}_r$ is the relative permittivity of the target. The total field inside the target is also a function of the contrast function of the target, making (1) become a complicated nonlinear equation which requires a long computation time and memory resources. In order to linearize the integral equation the first order Born approximation is employed. Under the first Born approximation, the total field inside the target can be approximated by the incident electric field

$$E_t\left(\rho, \rho_T, k\right) \cong E^{inc}\left(\rho, \rho_T, k\right) = ik\eta_0 G\left(\rho, \rho_T, k\right) \tag{3}$$

where η_0 is the wave impedance in the freespace $\eta_0 = 120\pi$. Substituting (3) into (1), the received scattered field can be written as

$$E_s\left(\rho_R, k\right) = i\eta_0 k^3 \int_{D_{inv}} G\left(\rho_R, \rho, k\right) G\left(\rho, \rho_T, k\right) \mathrm{O}\left(\rho\right) d\rho \tag{4}$$

The Green's function for the three layered background medium shown in Figure 1 can be expressed in the spectral form as the following Sommerfeld-like integral [18]

$$G\left(\rho_R, \rho, k\right) = \frac{i}{4\pi} \int_{-\infty}^{\infty} dk_x T\left(k_x\right) \frac{\exp\left(ik_x\left(x_R - x\right) + ik_{1z}\left(z_R - z\right)\right)}{k_{1z}} \tag{5}$$

where T is the transmission coefficient for the wall

$$T\left(k_x\right) = \frac{\left(1 - R_{12}^2\right)\exp\left(ik_{2z}d - ik_{1z}d\right)}{1 - R_{12}^2\exp\left(i2k_{2z}d\right)} \tag{6}$$

$$k_{1z}\left(k_x\right) = \sqrt{k^2 - k_x^2}, \quad k_{2z}\left(k_x\right) = \sqrt{k_2^2 - k_x^2}, \quad R_{12} = \frac{k_{1z} - k_{2z}}{k_{1z} + k_{2z}} \tag{7}$$

and where k_2 is the wavenumber in the wall.

It is noticed that the transmission coefficient in (6) only deals with a single layer homogeneous wall thus the DT algorithm in existing form is still not applicable to cinder block or reinforcement walls.

Substituting (5) into (4), one easily obtains

$$
\begin{aligned}
E_s\left(\rho_R, k\right) = &-\frac{i\eta_0 k^3}{16\pi^2} \int_{D_{inv}} \mathrm{O}\left(\rho\right) d\rho \iint dk_x dk'_x F\left(k_x\right) F\left(k'_x\right) \\
&\cdot \exp\left(i\left(k_x x_R + k'_x x_T\right) + i\left(k_{1z} z_R + k'_{1z} z_T\right)\right. \\
&\left. -i\left(k_x + k'_x\right) x - i\left(k_{1z} + k'_{1z}\right) z\right)
\end{aligned}
\tag{8}
$$

where $k'_{1z}(k'_x) = \sqrt{k^2 - k'^2_x}$, $k'_{2z}(k'_x) = \sqrt{k_2^2 - k'^2_x}$, the function $F(k_x)$ is given by

$$F\left(k_x\right) = \frac{\left(1 - R_{12}^2\right)\exp\left(ik_{2z}d - ik_{1z}d\right)}{\left(1 - R_{12}^2\exp\left(i2k_{2z}d\right)\right)k_{1z}} \tag{9}$$

For the monostatic radar system, it is noting that $x_R = x_T$, $z_R = z_T$, then (8) can be further written as

$$
\begin{aligned}
E_s\left(\rho_R, k\right) &= -\frac{i\eta_0 k^3}{16\pi^2} \int_{D_{inv}} O\left(\rho\right) d\rho \int \int dk_x dk'_x F\left(k_x\right) F\left(k'_x\right) \\
&\cdot \exp\left(i\left(k_x + k'_x\right) x_R + i\left(k_{1z} + k'_{1z}\right) z_R - i\left(k_x + k'_x\right) x \right. \\
&\left. -i\left(k_{1z} + k'_{1z}\right) z\right)
\end{aligned}
\tag{10}
$$

Let the spatial Fourier transform of the scattered field be $\tilde{E}_s(k_x, k)$, then we have

$$
\tilde{E}_s\left(k_x, k\right) = \int E_s\left(x_R, k\right) \exp\left(-ik_x x_R\right) dx_R
\tag{11a}
$$

$$
E_s\left(x_R, k\right) = \frac{1}{2\pi} \int \tilde{E}_s\left(k_x, k\right) \exp\left(ik_x x\right) dk_x
\tag{11b}
$$

Let $k''_x = k_x + k'_x$, from (10) and (11b) one can derive that

$$
\begin{aligned}
\tilde{E}_s\left(k''_x, k\right) &= -\frac{i\eta_0 k^3}{8\pi} \int_{D_{inv}} O\left(\rho\right) d\rho \int dk_x F\left(k_x\right) F\left(k''_x - k_x\right) \\
&\cdot \exp\left(-ik''_x x\right) \exp\left(i\left(k_{1z}\left(k_x\right) + k_{1z}\left(k''_x - k_x\right)\right) z_R\right) \\
&\cdot \exp\left(-i\left(k_{1z}\left(k_x\right) + k_{1z}\left(k''_x - k_x\right)\right) z\right)
\end{aligned}
\tag{12}
$$

When the target is in the far field of the radar, as $z \to \infty$ the inner Fourier integral in (12) can be efficiently evaluated with stationary phase method [14]. Similar to the derivation for the asymptotic evaluation of the Fourier integral in the appendix in [14], let $\Phi(k_x) = k_{1z}(k_x) + k_{1z}(k''_x - k_x)$, then the stationary point is given by

$$
\frac{\partial \Phi\left(k_x\right)}{\partial k_x} = -\frac{k_x}{k_{1z}} + \frac{k''_x - k_x}{k_{1z}\left(k''_x - k_x\right)} = 0
\tag{13}
$$

It can be derived from the above equation that the stationary point is presented at $k_x = \frac{k''_x}{2}$. It is interested to notice that the stationary point corresponds to the exploding reflection model [21]. Using the Taylor series expansion the phase item can be written as

$$
\Phi\left(k_x\right) \cong \Phi\left(k_{x0}\right) + \frac{1}{2}\Phi''\left(k_{x0}\right)\left(k_x - k_{x0}\right)^2
\tag{14}
$$

where k_{x0} is the stationary phase point and

$$
\Phi''\left(k_x\right) = -k^2 \left(\frac{1}{k_{1z}^3\left(k_x\right)} + \frac{1}{k_{1z}^3\left(k''_x - k_x\right)}\right)
\tag{15}
$$

By using the stationary phase formula in [11, 18], the inner integral in (12) can be asymptotically evaluated to yield the following expression

$$
\tilde{E}_s\left(k_x, k\right) = -\frac{i\eta_0 k^3}{8\pi} \int_{D_{inv}} d\rho \exp\left(-ik_x x\right) \mathrm{O}\left(\rho\right)
$$

$$
\cdot\sqrt{\frac{2\pi}{iz\Phi''\left(\frac{k_x}{2}\right)}} F^2\left(\frac{k_x}{2}\right) \exp\left(i2k_{1z}\left(\frac{k_x}{2}\right) z_R\right)
$$

$$
\exp\left(-i\left(2k_{1z}\left(\frac{k_x}{2}\right)\right) z\right) \tag{16}
$$

Then the relation between the spatial Fourier transforms of the scattered field and the contrast function can be simply derived from (16) and (17) as

$$
\tilde{E}_s\left(k_x, k\right) = -\frac{i\eta_0 k^3}{8\pi} \sqrt{\frac{2\pi}{i\Phi''\left(\frac{k_x}{2}\right)}} F^2\left(\frac{k_x}{2}\right) \exp\left(iz_R\sqrt{4k^2 - k_x^2}\right)
$$

$$
\tilde{\mathrm{O}}\left(k_x, \sqrt{4k^2 - k_x^2}\right) \tag{17}
$$

where the 2D spatial Fourier transform of $\mathrm{O}(\rho)/\sqrt{z}$ is given by

$$
\tilde{\mathrm{O}}\left(k_x, k_z\right) = \int_{D_{inv}} \frac{\mathrm{O}\left(\rho\right)}{\sqrt{z}} \exp\left(-ik_x x - ik_z z\right) d\rho \tag{18}
$$

Then the image can be efficiently reconstructed from its inverse Fourier transform with the following imaging formula

$$
\mathrm{O}\left(x, z\right) = \int \frac{i\sqrt{2z}}{\eta_0\sqrt{\pi^3}k^3} dk \int dk_x \tilde{E}_s\left(k_x, k\right) \exp\left(ik_x x\right) \sqrt{i\Phi''\left(\frac{k_x}{2}\right)}
$$

$$
\cdot F^{-2}\left(\frac{k_x}{2}\right) \exp\left(iz\sqrt{4k^2 - k_x^2} - iz_R\sqrt{4k^2 - k_x^2}\right) \tag{19}
$$

The above DT algorithm for TWRI can be efficiently implemented in the following steps:

1) Perform FFT to compute the spatial Fourier transform of the received scattered field $\tilde{E}_s(k_x, k)$ from (11a);

2) Compute the multiplication of $\tilde{E}_s(k_x, k)$ with $\sqrt{i\Phi''(\frac{k_x}{2})}F^{-2}(\frac{k_x}{2})$ then multiply it with the exponential factor $\exp(iz\sqrt{4k^2 - k_x^2} - iz_R\sqrt{4k^2 - k_x^2})$;

3) Apply IFFT at each down range pixel to evaluate the inner integral;

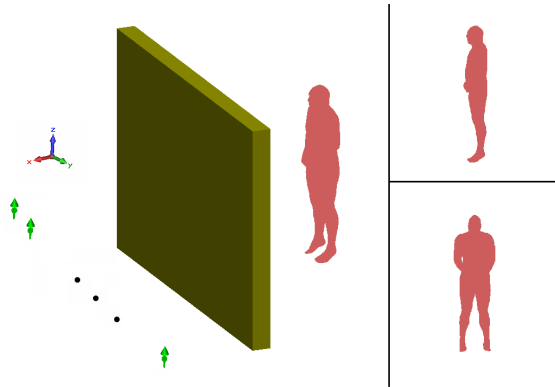4) Summation over all frequencies to calculate the outer integral.

Figure 2. Simulation geometry of a human behind the wall.

3. NUMERICAL AND EXPERIMENTAL RESULTS

In order to show the efficiency and effectiveness of the proposed DT algorithm for TWRI, some numerical and experimental results are presented in this section.

We first present a numerical result for the imaging of a human behind a single layer homogenous wall. The measurement configuration of the radar system is shown in Figure 2. The radar system scans the region of interest along a line parallel to the wall in the y direction at a distance of 0.3 m from the front wall. The length of the synthetic aperture is 2 m with an inter-element spacing 0.05 m. The dielectric constant, conductivity and thickness of the wall are $\varepsilon_r = 6$, $\sigma = 0.01$ S/m and $d = 0.2$ m. The measurement data was generated using XFDTD®, a commercial full wave electromagnetic simulator based on Finite Difference Time Domain (FDTD) method from Remcom Inc. The dimension of the HiFi male human model is 0.57 m $\times$ 0.324 m $\times$ 1.88 m and made up of 2.9 mm cubical mesh cells, 23 different tissue types with realistic dielectric and conductivity parameters. The front and side views of the human are shown at the top and bottom of the right side of Figure 2. The operating frequency of the radar ranges from 1 GHz–3 GHz with a step of 36 MHz. The investigation domain is a 2 m $\times$ 2 m square region and divided into 160×160 pixels.

Figure 3 is the imaging result of the human using the proposed DT TWRI algorithm. The approximate true region of the human is indicated with a white dashed ellipsoid which is 1.5 m behind the front boundary of the wall. From this figure we find that the human is clearly identified and is well located at the correct location. Through

the proper incorporation of the layered medium Green's function the wall effect has been well compensated and a high quality focused image of the target can be achieved by the proposed DT TWRI algorithm. For the convenience of comparison the imaging result using the DS beamforming algorithm in [8] is also presented in Figure 4, where the approximate true region of the human is also indicated with a white dashed ellipsoid. From Figures 3 and 4 it is clear that both the two algorithms are successful in imaging of the target without distortion or displacement of the target. It takes about only 0.647 s to reconstruct the image in Figure 3 using the proposed DT TWRI algorithm on a four-core P4 2.6 G desktop computer. However, it takes about 34.79 s to form the same size image in Figure 4 using the DS beamforming algorithm on the same computer. A significant acceleration, over a factor of 53, can be achieved using the proposed DT algorithm for TWRI.

Finally, an experimental study was carried out to examine the effectiveness and performance of the DT algorithm for TWRI. An ultra-wideband synthetic aperture through-the-wall radar system was set up in the lab-controlled environment. A stepped-frequency continuous wave (CW) signal, consisting of 201 frequency steps of size 12 MHz, covering the 0.7–3.1 GHz band was chosen for imaging. An Agilent vector network analyzer (VNA), model ENA 5071B, was used for signal transmission and data collection. A dual-polarized horn antenna, model ETS-Lindgren 3164-04, with an operational bandwidth from 0.7
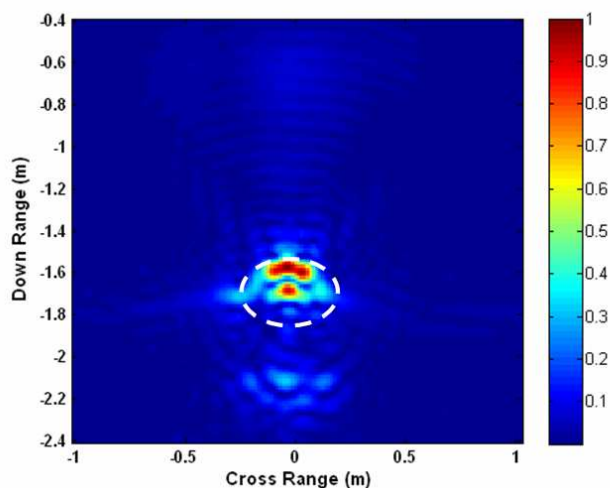

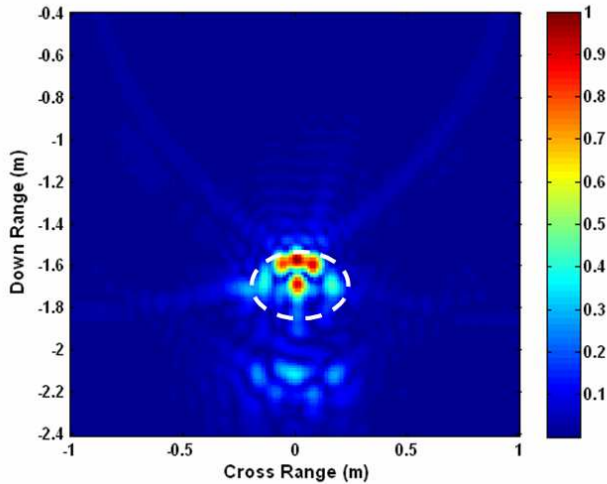**Figure 3.** Imaging result of the human with the proposed DT algorithm.

Figure 4. Imaging result of the human with DS beamforming algorithm.

to 6 GHz, was used as the transceiver and mounted on a Field Probe Scanner to synthesize a 57-element linear array with an inter-element spacing of 2.2 cm. The array is positioned 1.05 m in downrange from a 0.15 m thick solid concrete block wall with a dielectric constant of 7.66. Ports 1 and 2 of the network analyzer were connected to the V- and H-feeds of the antenna and full-polarization (VV, HH, HV and VH) measurements were conducted under monostatic measurement configuration. That is, the set of 201 CW frequencies is transmitted from a single array element and the returns are received at the same array location only. This process is then repeated for the next array location until all 57 array locations are exhausted. The scene, shown in Figure 5, consists of a dihedral (each face is 15.5 in high and 11 in wide) whose center is located 1.99 m behind the wall at a cross range of 0.285 m. Both the array and the center of the target were at the same height. An empty scene measurement was also made and was coherently subtracted from the target scene. The resulting datasets were used for generating the images.

Figure 6 provides the imaging result of the dihedral using the proposed DT TWRI algorithm. The true region of the target is indicated with a white dashed triangle in the image. From Figure 6 we find that the target is well located at the correct location. For comparison, the imaging result using the DS beamforming algorithm is provided in Figure 7. Although successful imaging results can be
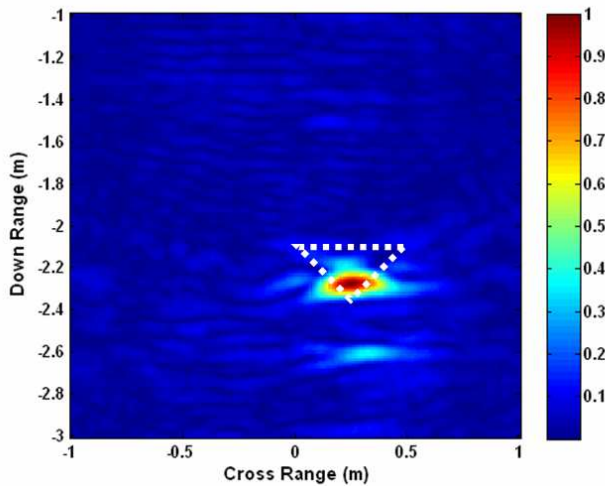
Figure 5. Scene being imaged.

Figure 6. Experimental result using the proposed DT algorithm.

obtained by using both algorithms, it takes only 2.75 s to generate the image in Figure 6 with the proposed DT algorithm while it takes about 70.16 s to form the same size image in Figure 7 using the DS beamforming algorithm on the same computer. The significant acceleration of the proposed DT algorithm for TWRI is achieved due to the following reasons:

(i) The coherent summation over all receiver locations in the linear inverse scattering algorithms and DS beamforming algorithm is efficiently computed with FFT in (11a), which reduces the beamforming time in the cross range.
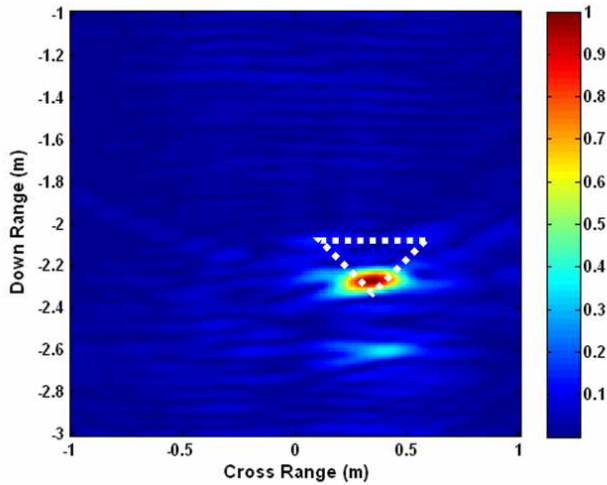
Figure 7. Experimental result using DS beamforming algorithm.

 (ii) The solving of the nonlinear equation in order to find the wave propagation path with ray tracing technique in the DS beamformer or the exact/approximate evaluation of the layered medium Green's function in the linear inverse scattering algorithms is avoided.
(iii) Instead of the pixel-by-pixel reconstruction in existing TWRI algorithms, the proposed DT algorithm reconstructs all the cross range pixels at each down range pixel with IFFT, which is much more efficient and less time consuming.

4. CONCLUSION

DT algorithm has been now widely used in its various forms for SAR imaging and GPR subsurface imaging due to the easy implementation with FFT/IFFT, which significantly reduces the computation time in the imaging. In this paper, a 2D DT algorithm based on the first order Born approximation is proposed for the imaging of hidden targets behind the wall. The background medium Green's function is incorporated to take into account the wall effect and to avoid the solving of a nonlinear equation required to find the wave propagation path with ray tracing technique. The spectral expansion of the three-layered background medium Green's function is employed to derive a linear relation between the spatial Fourier transforms of the image and the scattered field. The linearization of the inversion

scheme and easy implementation of the algorithm with FFT/IFFT make the DT algorithm suitable for on-site applications. Numerical and experimental results are presented to show the effectiveness and efficiency of the proposed DT algorithm for TWRI.

ACKNOWLEDGMENT

REFERENCES

1. Dehmollaian, M. and K. Sarabandi, "Refocusing through building walls using synthetic aperture radar," *IEEE Trans. Geosci. Remote Sensing*, Vol. 46, No. 6, 1589–1599, 2008.

2. Zhang, W., A. Hoorfar, and C. Thajudeen, "Polarimetric through-the-wall imaging," *2010 URSI International Symposium on Electromagnetic Theory (EMTS)*, 471–474, Berlin, Germany, 2010.

3. Dogaru, T. and C. Le, "SAR images of rooms and buildings based on FDTD computer models," *IEEE Trans. Geosci. Remote Sensing*, Vol. 47, No. 5, 1388–1401, 2009.

4. Muqaibel, A., A. Safaai-Jazi, A. Bayram, A. Attiya, and S. Riad, "Ultra-wideband through-the-wall propagation," *Proc. Inst. Elect. Eng.-Microw., Antennas Propag.*, Vol. 152, No. 6, 581–588, 2005.

5. Baranoski, E. J., "Through wall imaging: Historical perspective and future directions," *IEEE International Conference on Acoustics, Speech and Signal Processing*, 5173–5176, 2008.

6. Dogaru, T. and C. Le, "SAR images of rooms and buildings based on FDTD computer models," *IEEE Trans. Geosci. Remote Sensing*, Vol. 47, No. 5, 1388–1401, 2009.

7. Ahmad, F. and M. G. Amin, "Noncoherent approach to through-the-wall radar localization," *IEEE Trans. Aerospace and Electronic Systems*, Vol. 42, No. 4, 1405–1419, 2006.

8. Ahmad, F., M. G. Amin, and S. A. Kassam, "Synthetic aperture beamformer for imaging through a dielectric wall," *IEEE Trans. Aerospace and Electronic Systems*, Vol. 41, 271–283, 2005.

9. Soldovieri, F. and R. Solimene, "Through-wall imaging via a linear inverse scattering algorithm," *IEEE Geosci. Remote Sensing Lett.*, Vol. 4, No. 4, 513–517, 2007.

10. Song, L. P., C. Yu, and Q. H. Liu, "Through-wall imaging (TWI) by radar: 2-D tomographic results and analyses," *IEEE Trans. Geosci. Remote Sensing*, Vol. 43, No. 12, 2793–2798, 2005.

11. Zhang, W., A. Hoorfar, and L. Li, "Through-the-wall target localization with time reversal music method," *Progress In Electromagnetics Research*, Vol. 106, 75–89, 2010.

12. Wolf, E., "Three-dimensional structure determination of semi-transparent objects from holography data," *Opt. Commun.*, Vol. 1, 153–156, 1969.

13. Deming, R. and A. J. Devaney, "Diffraction tomography for multi-monostatic ground penetrating radar imaging," *Inverse Problems*, Vol. 13, 29–45, 1997.

14. Hansen, T. B. and P. M. Johansen, "Inversion scheme for monostatic ground penetrating radar that takes into account the planar air-soil interface," *IEEE Trans. Geosci. Remote Sensing*, Vol. 38, 496–506, 2000.

15. Cui, T. J. and W. C. Chew, "Novel diffraction tomographic algorithm for imaging two-dimensional dielectric objects buried under a lossy earth," *IEEE Trans. Geosci. Remote Sensing*, Vol. 38, 2033–2041, 2001.

16. Cui, T. J. and W. C. Chew, "Diffraction tomographic algorithm for the detection of three-dimensional objects buried in a lossy half space," *IEEE Trans. Antennas and Propagation*, Vol. 50, 42–49, 2002.

17. Lehman, S. K., "Superresolution planar diffraction tomography through evanescent fields," *Int. J. Imaging Systems Technol.*, Vol. 12, 16–26, 2002.

18. Chew, W. C., *Waves and Fields in Inhomogeneous Media*, Chapter 2, IEEE Press, Piscataway, NJ, 1997.

19. Soumekh, M., "A system model and inversion for synthetic aperture radar imaging," *IEEE Trans. Image Processing*, Vol. 1, 64–76, 1992.

20. Lopez-Sanchez, J. M. and J. Fortuny-Guasch, "3-D radar imaging using range migration techniques," *IEEE Trans. Antennas and Propagation*, Vol. 48, 728–737, 2000.

21. Li, L., W. Zhang, and F. Li, "A novel autofocusing approach for real time throughwall imaging under unknown wall characteristics," *IEEE Trans. Geosci. Remote Sensing*, Vol. 48, No. 1, 423–431, 2010.